Intrusion of Water in ZIF-8: Evidence of the Thermodynamic Instability under High Pressure

Amir Astafan, Céline Dirand, Andrey Ryzhikov, Habiba Nouali, T. Jean Daou, Claire Marichal, Jean-Pierre Bellat, Igor Bezverkhyy, Gérald Chaplais

Intrusion of Water in ZIF-8: Evidence of the Thermodynamic Instability under High Pressure

Amir Astafan,[a,b] Céline Dirand,[c] Andrey Ryzhikov,[a,b] Habiba Nouali,[a,b] T. Jean Daou,[a,b] Claire Marichal,[a,b] Jean-Pierre Bellat,[c] Igor Bezverkhyy,*[c] Gérald Chaplais*[a,b]

[a] *Université de Haute-Alsace, CNRS, Institut de Science des Matériaux de Mulhouse (IS2M), UMR 7361, Axe Matériaux à Porosité Contrôlée (MPC), F-68100, Mulhouse, France*

[b] *Université de Strasbourg, F-67000 Strasbourg, France*

[c] *Université de Bourgogne Franche-Comté, CNRS, Laboratoire Interdisciplinaire Carnot de Bourgogne, UMR 6303, F-21078 Dijon Cedex, France*

Abstract

High-pressure intrusion−extrusion experiments of water in hydrophobic zeolitic imidazolate framework (ZIF-8) were performed by two techniques: porosimetry and manometry coupled with calorimetry measurement. This study focuses on the variation of experimental duration (3−900 h) for both techniques in order to study the impacts of this parameter on the energetic performance of a “ZIF-8−water” system and the stability of ZIF-8. Prior to performing intrusion measurements, tests have been conducted in order to highlight that mechanical compression at 0.2 ton force to form pellets and outgassing at 473 K for 12 h under vacuum do not alter the structural and textural properties of starting ZIF-8 powder. The post-intruded samples have been characterized by X-ray diffraction, nitrogen sorption at 77 K, and scanning electron microscopy in order to evaluate the impact of experimental duration on the stability of the ZIF-8 framework. It has been observed that the duration of intrusion−extrusion tests affects system behavior. If the measurements’ duration is less than 4 days, the “ZIF-8−water” system acts as a molecular spring with fully reversible intrusion. In these conditions, the intrusion process is shown to be exothermic and the ZIF-8 framework is preserved. In contrast, for longer measurement durations, the system displays a combination of spring and bumper behaviors. This phenomenon is related to partial but gradual transformation of ZIF-8 into the nonporous ZIF-dia(Zn) phase. Complementary experiments have highlighted that both water and high pressure play crucial roles in this transformation of ZIF-8.

1. Introduction

The energy needs necessary to satisfy the development of the current social and economic model are constantly increasing. As a result, many alternative approaches have been developed in recent decades to replace fossil fuels while meeting the growing need for energy.[1] Energy storage is one of the most important challenges in this field.[2] More specifically, the storage of mechanical energy by intrusion−extrusion of nonwetting liquids into porous materials was discovered by Eroshenko.[3] In such systems, which are also called heterogeneous lyophobic systems (HLS), the energetic storage concept is based on the fact that to make a nonwetting liquid penetrate into the pores (intrusion), it is necessary to apply a higher pressure than the capillary one, which obeys the Laplace−Washburn equation

$$P = \frac{2\,\gamma\,cos\theta}{r_{pore}} \qquad (1)$$

where γ is the surface tension, r_{pore} is the radius of the pores, and θ is the contact angle between the liquid and the solid (θ >> 90°).

The mechanical energy E required to make the nonwetting liquid phase enter in solid pores is given by the relation

$$E = \int_{V_0}^{V_f} P.dV \qquad (2)$$

In this case, during the intrusion step, $E = E_s$ (the stored mechanical energy), $P = P_{int}$ (the intrusion pressure) and $V = V_{int}$ (the intrusion volume) which is also equal to the difference between V_f (the volume at the end of the volume variation step) and V_0 (the volume at the beginning of the volume variation step). When the pressure is released, the recovery of the mechanical energy occurs under extrusion of liquid out of the pores. Consequently, the terms displayed in eq 2 become $E = E_r$ (the restored mechanical energy), $P = P_{ext}$ (the extrusion pressure) and $V = V_{ext}$ (the extrusion volume) which is still expressed according to V_0 and V_f. Nevertheless, depending on material structure and composition as well as on the nature of the liquid, HLS can demonstrate spring, shock absorber, or bumper behavior by storing, dissipating, or absorbing the supplied energy, respectively. The first two behaviors correspond to fully reversible intrusion with small or large hysteresis between intrusion and extrusion curves, respectively, whereas the nonwetting liquid is not extruded for the bumper behavior. The energy supplied, in this case, is therefore not restored, but absorbed by the system.

A simplified version of eq 2 also exists and is often used to calculate the stored (E_s) / restored (E_r) / absorbed (E_a) energy of the HLS:

$$E = P.V \qquad \textbf{(3)}$$

where $E = E_s$ or E_a, $P = P_{int}$ and $V = V_{int}$, or $E = E_r$, $P = P_{ext}$ and $V = V_{ext}$

HLS were first developed from porous silica and liquid metals, then these two components were replaced by hydrophobic silica and water, a nonwetting and eco-friendly liquid.[4]

According to eq 2 (and eq 3 also), the higher the intruded volume and the intrusion pressure, the higher the stored mechanical energy. Furthermore, the intrusion pressure can be increased by using porous solids with a smaller pore diameter and higher hydrophobicity as highlighted in eq 1. It is to follow this strategy that, first, hydrophobic zeolites,[5-8] then Zeolitic Imidazolate Frameworks[9] have been used in pioneering works as porous matrices into HLS.[10]

Regarding zeolitic imidazolate frameworks (ZIFs), they are a subclass of metal−organic frameworks (MOFs), that include divalent metal ions (e.g., Zn^{2+}, Co^{2+}, $Cd^{2+}\cdots$) connected in an extended crystalline network by imidazolate-type linkers.[11] They have zeolite-related frameworks with various topologies due to the metal−linker−metal angle close to 145°, which is similar to the Si−O−Si angle in zeolites.[12,13] ZIFs have remarkably high pore volume and tunable surface properties that make them very interesting and promising materials for various applications such as gas storage,[14-17] liquid phase adsorption,[18-20] separation,[11, 21, 22] sensors,[23] and heterogeneous catalysis.[24] Owing to the concept of reticular chemistry offered by MOF-type materials,[25] it is possible to modulate the chemical composition of materials' frameworks (including their hydrophobic feature) while adapting their pore size and porous volume (toward a low aperture size and large volume, respectively, for the targeted application). In 2013, Ortiz et al. paved the way for their use in HLS by studying water intrusion−extrusion under high pressure in ZIF-8.[9] It has been shown that the behavior of this system was defined as spring with a stored energy of 13 $J{\cdot}g^{-1}$. Since then, the energetic performances of the same HLS or others based on different ZIFs have been further studied.[26-33] These studies have emphasized various effects of the crystal size and shape, the nature of the linker, and the topology and the nature of nonwetting liquid on the energetic performances of the investigated systems. ZIF-8 remains the most studied material, but most of the studies have been realized at room temperature and for a short experimental duration.[26, 28, 30, 34, 35]

ZIF-8 is generally considered to be stable in air and in water.[12] However, Liu et al. described that hydrothermal treatment at low mass ZIF-8/H_2O ratio leads to the collapse of ZIF-8 crystalline structure and formation of ZnO.[36] Yin et al. noted that the ZIF-8 structure is less stable in a steam atmosphere than in argon and air at high temperature (673 K). Moreover, Grosu et al. have shown that water intrusion− extrusion cycles at 360 K under high pressure leads to irreversible modification of the ZIF-8 structure consisting of a loss of symmetry from cubic to orthorhombic.[35] More recently, James et al. reported that the ZIF-8 structure is preserved after treatments (20 h at 473 K) in inert, oxidizing, and reducing environments.[37] In the work of Zhang et al., it was found that the ZIF-8 material degrades in water at room temperature after 72 h of immersion time and that the degradation rate increases with decreasing the mass ratio of ZIF-8 to water.[38, 39] Besides, it was recently highlighted that ZIF-8 is not stable at temperatures below 573 K in the presence of air. The material undergoes hydrolysis which leads to a novel pseudo-polymorph of ZIF-8.[40] At last, ZIF-8 has been used in a diamond anvil cell through high-pressure experiments using water, methanol, ethanol, CO2, SF_6, or $CHClF_2$ as pressure transmitting media (PTM).[41-43] ZIF-8 shows pressure- induced amorphization in SF_6 but remains crystalline with water under a pressure of 2.16 GPa. Thus, the thermal stability of ZIF-8 in addition to the one regarding the contact with aqueous solutions is a matter of debate.

On another note, few data have been reported about the thermal energy of intrusion of water in this MOF-type material. The determination of the intrusion heat of water in porous materials such as zeolites and mesoporous silica has been performed by Coiffard et al. and Karbowiak et al.[44, 45] These authors have developed their own apparatus combining calorimetry and manometry to measure the thermal effects during intrusion. The intrusion calorimetry technique provides rich information about the intrusion process. For example, it has been shown that the intrusion process in zeolites can be endothermic or exothermic depending on the pore geometry and interaction with silanol defects.[46] Thermal energy is not negligible compared to mechanical one. The evolution of the intrusion heat during successive intrusion−extrusion cycles shows whether the material undergoes some modifications during the intrusion−extrusion process.[45, 47] Concerning ZIF-8, to the best of our knowledge, Grosu et al. are the only authors to have studied the intrusion of water in this well-known material by calorimetry.[35] They found that the intrusion of water is endothermic with a value of the

intrusion heat of around 4 $J \cdot g^{-1}$ at 300 K. Nevertheless, no calorimetric data obtained after several intrusion−extrusion cycles are given.

All data reported in the literature about the intrusion of water in ZIF-8 are not sufficient for having a clear and detailed understanding of the intrusion−extrusion process. In partic- ular, the thermodynamic stability of ZIF-8 in the presence of water for several long intrusion−extrusion cycles has not been established. As mentioned above, contradicting conclusions about the stability of ZIF-8 were drawn according to the effect of water and contact duration. Kinetics seems to play an important role, but it has not been studied up to now. Furthermore, the thermal effects occurring during intrusion− extrusion cycles have not been studied in detail.

The present work is therefore devoted to the study of the intrusion−extrusion of water in ZIF-8 at room temperature by using intrusion porosimetry and in situ calorimetry, with particular emphasis on the stability of the material. To achieve this goal, successive intrusion−extrusion cycles were performed by altering the cycle duration in a wide range and the properties of the post-intruded ZIF-8 samples were characterized in detail.

2. Methods

2.1. Materials

2.1.1. Reactants, Additive and Solvent

Zinc nitrate hexahydrate ($Zn(NO_3)_2 \bullet 6H_2O$, 99%), 2-methylimidazole ($C_4H_6N_2$, Hmim, 97%) and aqueous solution of ammonia (NH_3, 32%) were bought from Alfa Aesar, ABCR and Roth, respectively, and used without further purification. Methanol (MeOH, 99.9%) was provided by Carlo Ebra and deionized water was used.

2.1.2. Syntheses of ZIF-8 Powder

The synthesis protocol was readjusted from the one supplied by He et al.[48] with modifications concerning quantities (ca. 48 times up-scaling) and recovering of material (filtration instead of centrifugation) process.

Briefly, 28.7 g (96.5 mmol) of $Zn(NO_3)_2 \bullet 6H_2O$ are dissolved in 162.6 g (9023 mmol) of deionized water in a glass beaker and stirred at 500 rpm for 18 minutes to give a solution (Solution 1). At the same time, 15.7 g (191.7 mmol) of 2-methylimidazole (Hmim) are mixed in 163.9 g (3080 mmol) of aqueous ammonia in a glass flask, and stirred at 1000 rpm for 10 minutes to form a solution (Solution 2). Then, Solution 1 is poured in an addition ampoule and added in 1 minute to Solution 2 under stirring at 500 rpm. The mixture composition is 1 $Zn(NO_3)_2$: 2 Hmim : 32 NH_3 : 164 H_2O. The stirring conditions are maintained for 10 minutes in order to obtain a white suspension before stopping. A white solid is recovered by filtration, washed with deionized water (2880 mL by portions of 40 mL) in order to decrease the filtrate pH to ~ 8. The solid is soaked in 400 mL of MeOH for 2 hours and recovered by centrifugation at 7000 rpm for 15 minutes after elimination of the supernatant. This activation stage is repeated three times under the same conditions. The last stage consists of redispersing the recovered material in MeOH to get a final suspension and performing filtration before drying the solid overnight under air and at room temperature. 10.1 g of crystalline, white, and dried powder are collected with a yield of 46 %

2.1.3. Preparation of ZIF-8 Pellets

Around 100 mg of ZIF-8 material are outgassed at 423 K for 1 h then compacted by using a hydraulic press (at 0.2 ton force) into a self-supported pellet (1 cm of diameter) during 2 min in order to limit

the volume variation under intrusion−extrusion experiments related to powder compacting and intergranular porosity filling.

2.2. Characterization Techniques

The samples obtained after intrusion−extrusion experiments were characterized in the two different laboratories involved in the present study. The porosimetry measurements were performed at the Institut de Science des Matériaux de Mulhouse (IS2M) and the ZIF-8 samples collected after these measurements were characterized in this laboratory. The calorimetric measurements were realized in Laboratoire Interdisciplinaire Carnot de Bourgogne (ICB) and the corresponding samples were characterized in this laboratory. For this reason, the analyses conditions of each technique used in the two laboratories are listed in the next paragraphs.

2.2.1. Powder X-Ray Diffraction

X-ray diffraction patterns of the starting samples and the ones collected after porosimetry were recorded in transmission mode on an STOE STADI-P diffractometer equipped with a curved germanium (111), primary monochromator, and a linear position-sensitive detector (6° in 2θ) using Cu $K_{\alpha 1}$ radiation (λ = 1.5406 Å). Measurements were achieved for 2θ angle values in the 5−50° range, with a step of 0.04° in 2θ.

The X-ray diffraction (XRD) measurements for the samples after calorimetry experiments were realized in reflection mode in the range of 3−50° (in 2θ) with a diffractometer Bruker D8-A25 Discover equipped with a LynxEye XE detector using a nonmonochromatic Cu K_{α} radiation.

2.2.2. Nitrogen Adsorption-Desorption Measurements

The nitrogen adsorption−desorption isotherms of the starting samples and the ones collected after porosimetry were carried out at 77 K using a Micromeritics ASAP 2420 setup. Prior to the adsorption measurements, the samples were outgassed at 473 K during 12 h under vacuum. Brunauer−Emmett−Teller surface areas, denoted as S_{BET}, were calculated in a $0.0004 \leq p/p^0 \leq 0.004$ range for all materials in agreement with the criteria given in the literature.[49] The microporous volumes (V_{μ}) were determined using the *t*-plot method (Harkins and Jura model).

The nitrogen adsorption−desorption isotherms of the samples after calorimetry experiments were measured using ASAP 2020 equipment from Micromeritics. The solids were degassed for 15 h at

473 K before measurements. The same treatment conditions as previously mentioned were followed to determine the surface area and the microporous volume.

2.2.3. Thermogravimetric Analyses

For all samples, TGA measurements were performed on a TG Mettler Toledo STARe apparatus, under an air flow, with a heating rate of 2 $K \cdot min^{-1}$ from 300 to 1173 K.

2.2.4. Scanning Electron Microscopy

The size and the shape of ZIF-8 particles were determined using a JEOL JSM-7900F scanning electron microscope equipped with an energy-dispersive X-ray spectrometer composed of two XFlash 6−30 X-ray detectors from Bruker (Billerica). Before analysis, the samples were sputter coated with gold in order to provide sufficient resolution to observe the fine structure of materials. Scanning electron microscopy (SEM) images were acquired using an in-lens electron detector.

2.2.5. Water Intrusion-Extrusion Experiments (Porosimetry)

The intrusion−extrusion experiments have been performed at room temperature over three cycles using a modified mercury porosimeter (Micromeritics Model Auto-pore IV).[50] Typically, around 100 mg of pelletized ZIF-8 and around 500 mg of water are directly introduced in the polypropylene cylinder cell of 2 mL capacity and sealed. This cell is introduced in the 15 mL glass cell of the porosimeter which is filled with mercury. The values of the intrusion (P_{int}) and extrusion (P_{ext}) pressures are determined from the incremental pressure variation. Pressure is expressed in megapascals (MPa) and volume in milliliters per gram of sample ($mL \cdot g^{-1}$). The intruded and the extruded volumes (Vint, Vext) correspond to volume variations between the beginning and the end of each step (intrusion and extrusion). The stored (restored) energy (E_s or E_r) corresponds to the product of the pressure and volume according to eq 3. In this study, the energetic behavior of an HLS is classified as a shock absorber or spring based on a complete extrusion of the intruded liquid from the solid with an energy yield (E_r/E_s) lower or higher than 80%, respectively. It should be noted that the impact of the shaping of ZIF-8 powder in pellet form on the pressures and volumes of intrusion and extrusion have been studied before using the pellets for the intrusion−extrusion experiments aiming to investigate the influence of experimental duration (Section 3.1). In this case, the maximum pressure of around 100 MPa was achieved along 3 cycles of around 3 h each leading to a whole duration of 9 h. Main experiments of deionized water intrusion−extrusion with different

experimental duration: 2 days, 3 days, 4 days and 9 days have been carried out on pellets of ZIF-8 material in order to determine how the duration of cycles impacts the intrusion−extrusion characteristics and ZIF-8 stability. An additional study of intrusion−extrusion (compression−decompression) with oil (Micromeritics high-pressure fluid, Ref: 920/16001/00) for 9 days of duration has been performed in order to study the influence of high pressure on ZIF-8 stability in the absence of water.

After water intrusion−extrusion experiments, all the samples were recovered by filtration, washed with 100 mL of deionized water, and then dried under air at room temperature overnight. ZIF-8 samples after oil intrusion−extrusion (compression−decompression) experiments were soaked in 100 mL of diethylether (DEE) overnight, followed by a sonication during 30 min, filtration, washing with 100 mL of DEE and drying under ambient air overnight.

2.2.6. Water Intrusion-Extrusion Experiments (Calorimetry)

The heat released during the intrusion and extrusion of water have been measured with a home-made apparatus combining calorimetry and high-pressure manometry (Figure S1). This device is similar to the one described in detail in a previous work.[45] Basically, it is composed of a Setaram C80 differential calorimeter equipped with specific vessels supporting high fluid pressure (up to 400 MPa). The calorimetric vessel containing the sample is directly connected to the manometric device containing water and equipped with a hand pump that allows compressing the liquid water to the desired pressure. The reference vessel is filled with water and maintained at atmospheric pressure. The displacement of the pump piston can be measured with a dial indicator to follow the variation of the fluid volume at the condition that the displacement is slow enough (slow compression). Thus, it is possible, after correction for the water compressibility to assess the volume of intruded water. The mass of the sample used is around 0.5 g. Prior to experiments, it is outgassed *in situ* under primary vacuum at room temperature for about 10 min. Then, water is introduced and measurements are performed at 298 K in the pressure range 1−50 MPa, or even 200 MPa in some cases.

Two experimental procedures are used to characterize the thermal effect of intrusion or extrusion (Figure S2). The first one is to rapidly compress the liquid water up to the final pressure (50 MPa). In this case, the integration of the calorimetric signal directly gives the integral heat of interaction of water with the solid

$$Q_{wz,int} = \frac{1}{m}\left(Q_{calo} - Q_{liquid}\right) \quad (4)$$

with Q_{calo} the integral calorimetric heat and Q_{liquid} the integral heat of compression of liquid water.

The final pressure is reached in 2 min and maintained for 1 h 30 min before returning to the initial one (this time is necessary for the calorimeter to go back to its steady state). Thus, an intrusion−extrusion cycle is performed in 3 h. These experiments are referenced as “fast procedure” in the following. The second procedure consists in increasing the pressure in successive increments of around 2 MPa up to the final pressure. At each pressure increment, the heat flux given by the calorimeter is integrated along time to obtain the calorimetric differential heat δQ_{calo}. Then, the differential heat of water/ ZIF-8 interaction $\bar{Q}_{wz,int}$ is calculated using the equation

$$\bar{Q}_{wz,int} = \frac{1}{m}\left(\frac{\delta Q_{wz,int}}{dP}\right)_T = \frac{1}{m}\left(\frac{\delta Q_{calo}}{dP} - \frac{\delta Q_{liquid}}{dP}\right)_T \quad (5)$$

where m is the mass of sample, dP is the pressure increment and δQ_{liquid} is the heat of compression of liquid water. The integral heat of water/ZIF-8 interaction is given by

$$Q_{wz,int} = \int_{\Delta P_{int}} \left(\frac{\delta Q_{wz,int}}{mdP}\right)_T dP \quad (6)$$

where ΔP_{int} is the pressure domain of intrusion.

This differential method takes time and requires at least 1 h 30 min for each pressure increment. Thus, one intrusion−extrusion cycle takes about 300 h (12.5 days). In the following, this type of experiments will be referenced as a “slow procedure”. For both fast and slow procedures, the same calculations are used for extrusion when the pressure is reduced after intrusion.

The heat released during compression of liquid water (Q_{liquid} or δQ_{liquid}) is determined by performing blank experiments in the same conditions, but without solid. As these calibrations are performed using a sample vessel of volume V_c (V_c = 1.4 mL) filled only with water, it is necessary thereafter to account for the volume occupied by the solid. For the fast procedure, as the variation of pressure exceeds the intrusion pressure, the heat of liquid compression given by blank experiments is multiplied by the ratio $\frac{V_c - V_s}{V_c}$ with V_s the volume of the solid framework. For the slow

procedure, the heat of liquid compression is corrected before intrusion by the ratio $\frac{V_c - V_s - V_\mu}{V_c}$, with V_μ the micropore volume, and after intrusion by the ratio $\frac{V_c - V_s}{V_c}$. We assume here that the intruded water has the same compression heat as the liquid water. That may not be true in general, but since the volume of the intruded water (~ 0.2 mL) is much lower than that of the sample vessel, such an assumption should not influence the obtained value of heat of interaction. It may be noticed that the heat of water/ZIF-8 interaction ($Q_{\mathrm{wz,int}}$) is not the heat of intrusion. It takes into account other thermal effects than the surface wetting, for example, the compression of the intruded and solid phases or the change in the density of water when it is intruded.

3. Results and Discussion

3.1. Influence of Compression and Outgassing of ZIF-8 Samples on the Energetic Properties of the "ZIF-8−water" System

The use of ZIF-8 pellets in the evaluation of energetic performance of the "ZIF-8−water" system is expected to decrease the impact of interparticular volume and to facilitate the placing of the sample and water in the polypropylene cylinder cell. Several ZIF-8 pellets were prepared by compression of ZIF-8 powder at 0.2 ton force for 2 min. The starting white crystalline powder and pellets were outgassed at 473 K for 12 h in some cases in addition.

3.1.1. Characterization of Parent ZIF-8 Powder and Pellets

The ZIF-8 parent powder and prepared pellets were characterized by XRD and N_2 adsorption−desorption. The XRD patterns of both types of materials are reported in Figure S3 and are similar to the simulated one (referenced with CCDC number 823083 and RefCode OFERUN02[51]). The structure and the crystallinity of ZIF-8 shaped as a pellet is thus preserved despite the mechanical constraint. The N_2 adsorption−desorption isotherms at 77 K of powder and pellet samples are given in Figure S4. Both isotherms display the typical profile of ZIF-8 isotherm characterized by a hysteresis at low relative pressure.[52-54] Table S1 summarizes the textural properties of powder and pellet materials and also confirms that the textural properties of ZIF-8 after compression remain similar. Figures S5 and S6 display TG curves and SEM images of the ZIF-8 parent powder and highlight, on the one hand, the absence of occluded molecules in the porosity as well as the hydrophobic feature of ZIF-8, and, on the other hand, the submicrometric size and the cubic shape with truncated edges of the ZIF-8 particles.

Water intrusion−extrusion experiments were then performed on powder and pellet samples in order to evaluate the influence of compressibility and outgassing on both the energetic properties and the stability of ZIF-8 material.

3.1.2. Pressure-Volume Diagrams

The Pressure−Volume (P−V) diagrams, obtained during three successive water intrusion−extrusion cycles (with pressure up to 100 MPa and 3 h for each cycle), are given in Figure S7. For the three cycles, ZIF-8 powder exhibits an intrusion pressure (P_{int}) around 27 MPa and an intruded volume (V_{int}) of 0.40 mL·g^{-1} (Table S2). The extrusion pressure (P_{ext}) is around 24 MPa and the extruded

volume (V_{ext}) equals 0.40 mL·g^{-1} for the three cycles. These parameters remain the same regardless of the conditions of pretreatment (pelletization and outgassing at 473 K under vacuum) for all cycles. For all used pretreatment conditions, the water intrusion−extrusion process is completely reversible with a small hysteresis making investigated "ZIF-8−water" systems molecular springs with stored energies close to 11 J·g^{-1} (Table S2). Consequently, both the compression of ZIF-8 powder into pellets and the outgassing at 473 K under vacuum do not affect the energetic properties of "ZIF-8−water" system.

3.1.3. Characterization of Post-Intruded Materials

All samples of ZIF-8 before (Section 3.1.1) and after intrusion−extrusion experiments were characterized by XRD and N_2 adsorption−desorption at 77 K. For all post-intruded ZIF-8 samples, both the structure (Figure S8) as well as the textural properties (Figure S9 and Table S3) are essentially preserved. An additional peak with a very low intensity is observed at around 11° (2θ) in some of XRD patterns. This could be assigned to a structural disorder rather than chemical change leading to a doubling of ZIF-8 conventional lattice (see also Section 3.2.3.1). Hence, it can be concluded that the ZIF-8 framework is stable after three water intrusion−extrusion cycles up to 100 MPa for a total experimental duration of 9 h.

3.2. Impact of Experimental Duration on the Energetic Properties of "ZIF-8−water" System

3.2.1. Pressure-Volume Diagrams (Porosimetry)

Several experiments of water intrusion−extrusion in ZIF-8 (by using pellets prepared from outgassed powder) have been performed in a pressure range of 1 to 100 MPa with different experimental duration for three cycles: 9 h (the duration used in all our previous studies), 2, 3, 4 and 9 days. The pressure−volume (P−V) diagrams of three successive intrusion−extrusion cycles are shown in Figure 1 and characteristic data are reported in Table 1. The low-pressure range (below 5 MPa) is not reported because it corresponds to the filling of intergranular porosity.[9, 26, 27]

The most important impact of experiment duration is observed for the reversibility of the intrusion−extrusion process, and thus for the intruded volume (V_{int}) evolution during cycling. For the shortest duration (i.e., 9 h), the intrusion is entirely reversible, the intruded and extruded (V_{ext}) volumes remain the same for all three cycles. This corresponds to the spring behavior. The

intrusion−extrusion curves and corresponding characteristics are very close to those observed in our previous works. [9, 28, 30] For longer experiments (*i.e.*, 2 and 3 days), like the shortest duration, the intrusion is fully reversible, the intruded volume remains constant for all cycles and a spring behavior is observed. It is also worth noting that for the experiment of 4 days, the intruded volume decreases slightly by 0.03 mL·g^{-1} (from the first to the third cycle) while for the experiment with 9 days, this evolution, more marked, achieves 0.12 mL·g^{-1}. In these two cases, the system thus displays a combination of spring and bumper behavior, the latter being more pronounced for the longest duration.

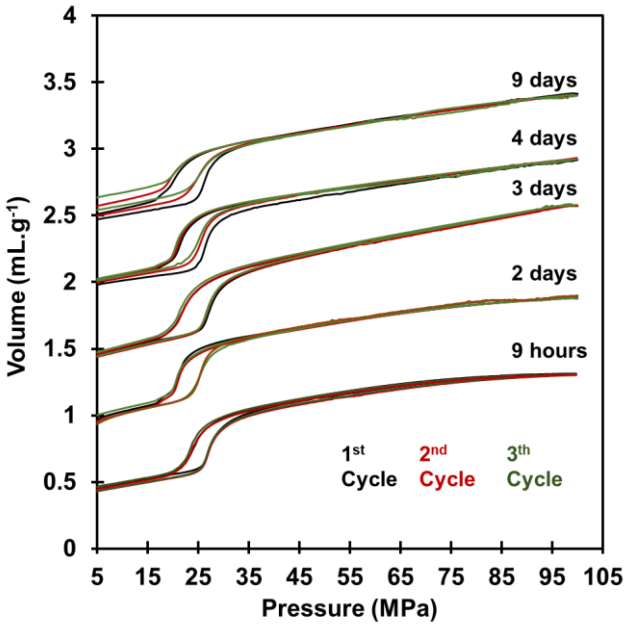

Figure 1. Intrusion−extrusion curves (pressure−volume diagrams) of the "ZIF-8−water" system with different experimental durations. For better visibility, the diagrams are shifted by 0.5 mL·g^{-1} along the *y*-axis.

Regarding the intrusion pressure (Pint) for the first cycle, it lies between 26 and 27 MPa regardless of the experiments' duration, while for both the second and the third cycles, a slight decrease of ~1 MPa is observed for the longest tests of water intrusion−extrusion (4 and 9 days) (Table 1). However, the extrusion pressure (P_{ext}) decreases more with experiment duration (by ~2.5 MPa for 2, 3 and 4 days tests and by ~3.5 MPa for the 9 days) compared to 9 h duration.

Table 1. Characteristics of the "ZIF-8−Water" System after Several Intrusion−Extrusion Experiment Durations: Intrusion (P_{int}) and Extrusion (P_{ext}) Pressures, Intruded (V_{int}) and Extruded (V_{ext}) Volumes, and Stored (E_s) and Restored (E_r) Energies

Experiments Duration		P_{int} (MPa)	P_{ext} (MPa)	V_{int} (mL·g^{-1})	V_{ext} (mL·g^{-1})	E_s (J·g^{-1})	E_r (J·g^{-1})
9 hours	Cycle-1	26.9	23.4	0.40	0.40	10.8	9.4
	Cycle-2	26.9	23.4	0.40	0.40	10.8	9.4
	Cycle-3	26.9	23.4	0.40	0.40	10.8	9.4
2 days	Cycle-1	26.0	21.0	0.40	0.40	10.4	8.4
	Cycle-2	26.0	21.0	0.40	0.40	10.4	8.4
	Cycle-3	26.0	21.0	0.40	0.40	10.4	8.4
3 days	Cycle-1	26.9	21.4	0.40	0.40	10.8	8.6
	Cycle-2	26.9	21.4	0.40	0.40	10.8	8.6
	Cycle-3	26.9	21.4	0.40	0.40	10.8	8.6
4 days	Cycle-1	26.4	20.5	0.40	0.37	10.6	7.6
	Cycle-2	25.5	20.5	0.37	0.37	9.4	7.6
	Cycle-3	25.5	20.5	0.37	0.37	9.4	7.6
9 days	Cycle-1	26.5	20.0	0.40	0.34	10.6	6.8
	Cycle-2	25.5	20.0	0.34	0.28	8.7	5.6
	Cycle-3	25.5	20.0	0.28	0.20	7.1	4.0

Concerning the stored energy (Es), for the first cycle, it remains unchanged regardless of the experiment duration (around 10.5 J·g−1). From 4 days of experiment duration the stored energy for both the second and third cycles decrease. The restored energy (Er) decreases also with the increasing of experiment duration for the three cycles. As described above, the mechanical energy (Es or Er) corresponding to the product of the pressure and volume, consequently an expected decrease occurs from 4 days of experiment duration essentially due to notable decrease of the intruded volume.

3.2.2. Intrusion-Extrusion Calorimetry (Thermal Energy)

3.2.2.1. Fast Intrusion-Extrusion Experiment (3 hours of Experiment Duration)

The heats measured during a first fast or slow compression−decompression cycle are given in Table 2. They are expressed in joule per gram of solid. The volumes of water intruded and extruded, which are also reported, are those determined from the experiments performed with the slow procedure. They are given by the jump of volume observed on the *P*−*V* diagram when intrusion or extrusion occurs (this jump of volume is not detectable with our apparatus when the fast intrusion−extrusion method is used). The *P*−*V* diagram obtained with the calorimetric apparatus is the same as the one obtained by porosimetry (Figure 1). From this volume variation, considering that the water which leaves the liquid phase is that which enters the pores, the heat of water/ZIF-8 interaction can be

calculated in joule per mole of intruded water taking for the liquid phase at 298 K a density equal to 1.00677 and 1.00887 g·mL^{-1} at 20.9 and 27.0 MPa, respectively.[55] It may be noticed that the thermal energy (Qwz,int) released during the compression process is not negligible. It represents up to 60% of the mechanical energy stored in the system and 37% of the total energy exchanged with the environment. Thus, the intrusion of water in ZIF-8 is also a way to store thermal energy.

Table 2. Heats of Water/ZIF-8 Interaction and Volumes of Intruded Water in ZIF-8 Determined by Calorimetry Coupled with Manometry during a First Fast and Slow Intrusion−Extrusion Cycle.[a]

Experiments Duration	P_{int} (MPa)	P_{ext} (MPa)	V_{int} (mL.g^{-1})	V_{ext} (mL.g^{-1})	$Q_{wz,int}$ (J.g^{-1})	$Q_{wz,ext}$ (J.g^{-1})	$Q_{wz,int,m}$ (J.mol^{-1})	$Q_{wz,ext,m}$ (J.mol^{-1})
3 hours	26.4	18.0			-6.5	5.4	-	-
12.5 days	27.0	20.9	0.41	0.33	-5.2	2.7	-226.3	146.3

[a] The pressure variation is 50 MPa. $Q_{wz,int}$ and $Q_{wz,ext}$ are given in Joule per gram of ZIF-8 (J·g^{-1}). $Q_{wz,int,m}$ and $Q_{wz,ext,m}$ are given in Joule per mol of intruded water (J·mol^{-1}).

Results obtained from the first fast compression−decompression cycle show that the intrusion process is exothermic with a heat of water/ZIF-8 interaction (Qwz,int) of −6.5 J·g^{-1}. This result is in contradiction with that reported by Grosu et al. who found that the intrusion is endothermic with a value of 4.4 J·g^{-1}.[35] Nevertheless, the intrusion pressure is in good agreement with the value reported by these authors as well as those measured by Ortiz et al. and evaluated by porosimetry (*i.e.*, 26.4 against 24.6,[35] 26.6,[9] and 26.9 MPa (Section 3.2.1), respectively). The difference between our heat of water/ZIF-8 interaction and that determined by Grosu et al. is 10.9 J·g^{-1} in absolute value which is difficult to explain. We suggest that the following reasons can be proposed: (i) the calorimetric technique employed by Grosu et al. is different from the ours and they do not specify which corrections were made to the measured calorimetric heat; (ii) the sample used by Grosu et al. is a commercial material purchased from Aldrich (Basolite Z1200) for which the preparation and activation procedures are not reported; (iii) their compression speed (1 MPa·min^{-1}) was much lower that the used in our fast procedure (25 MPa·min^{-1}); (iiii) the duration of their compression−decompression cycles was shorter (90 min against 180 min in our study). We know that all these parameters can have an impact on the energy involved in water intrusion. We carried out a number of experiments by modifying the pressure range studied or the compression speed on different batches of samples. In these experiments, some variations were indeed observed (~10%

of the measured values), but they never reached such a magnitude. The heat involved during decompression are given in absolute value and the extrusion pressure are lower than corresponding values related to intrusion. Grosu et al. and Ortiz et al. also found a lower extrusion pressure (between 18[35] and 22[9] MPa). The same is true with our measurements carried out by porosimetry (23 MPa).

3.2.2.2. Slow Intrusion-Extrusion Experiment (12.5 days of Experiment Duration)

Figure 2 shows the global heat measured by calorimetry (Q_{calo}) and the heat due to the compression of the liquid (Qliq) involved during the intrusion process by following the slow procedure. The heat of water/ZIF-8 interaction ($Q_{wz,int}$), obtained by subtracting these two values, is also reported. Results show again that the intrusion process is exothermic (Table 2). It may be noticed that the heat of water/ZIF-8 interaction related to one intruded water molecule ($Q_{wz,int,m}$) is very low compared to the net adsorption heat of water ($\Delta H_{vaporisation} + \Delta H_{gas\ adsorption}$) which is of a few $kJ \cdot mol^{-1}$ in hydrophobic materials like silicalite-1 for example (around 14 $kJ \cdot mol^{-1}$).[47] This means that the interaction of water with ZIF-8 is very weak compared to that of water with siliceous zeolites. Thus, ZIF-8 exhibits a very strong hydrophobic character. Though the heat of water/ZIF-8 interaction is of the same order of magnitude as for fast compression, the heat involved during decompression is much lower. This effect suggests that intrusion−extrusion process of water in ZIF-8 is irreversible. This conclusion is further supported by the results of three successive slow compression−decompression cycles. The results show that after the third cycle, corresponding to a total contact time with water greater than 600 h, the heat involved during intrusion is only $-3.1\ J \cdot g^{-1}$ and no heat is detectable during extrusion (Table S4). Therefore, it can be concluded from all these results that the porous solid is likely to undergo structural and/or chemical changes already after the first long-duration intrusion experiment.

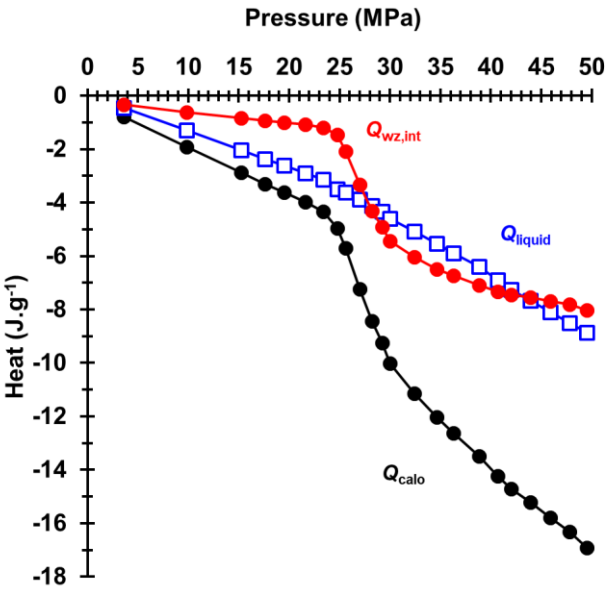

Figure 2. Integral heats of water interaction with ZIF-8 determined from slow procedure intrusion experiments ($Q_{wz,int} = Q_{calo} - Q_{liquid}$).

3.2.2.3. Effect of the Final Pressure on the Thermal Energy

The fast intrusion experiments discussed above are all performed in the range 1−50 MPa. Furthermore, additional intrusion runs have also been carried out up to higher final pressures (200 MPa). Results are shown in Figure S10 depicting the integral heat of interaction of water with the solid $Q_{wz,int}$ as a function of the final pressure. As the intrusion pressure determined from the $P-V$ diagram is 26.9 MPa, no thermal effects should occur below and above this pressure. Hence, $Q_{wz,int}$ should be zero below 26.9 MPa and −6.5 $J \cdot g^{-1}$ above. Nevertheless, this is not what was observed: above 26.9 MPa, $Q_{wz,int}$ continuously decreases with the final pressure. The same result is observed when a slow intrusion−extrusion experiment is performed. The heat integrated from the initial pressure to the final pressure (eq 4) continuously decreases after intrusion. Moreover, this value is not null before intrusion (Figure 2). This means that another thermal exothermic effect is present during the compression phase. This effect can be attributed to the compression of the ZIF-8 structure. It may also be due, after intrusion, to the compression of the intruded water which could be in a different physical state than the bulk liquid. As this exothermic effect is also observed before intrusion, it is probably due to the compression of the ZIF-8 framework. It is worth noting that such a phenomenon has never been observed in zeolites whose structures are much more rigid than those of MOFs to which ZIF-8 belongs. Thus, the relative flexibility of the ZIF-8 structure appears to play a

role in the intrusion process of water, at least from a thermal energy perspective. This result is in line with those of the literature which provided the evidence of ZIF-8 framework flexibility upon pressure-induced liquid intrusion.[32, 56, 57] According to these authors, such a framework flexibility would be accommodated by a gate-opening mechanism progressively induced by the rotation (swing) of the imidazolate linkers.

3.2.3. Characterization of Post-Intruded Materials

All our results obtained by porosimetry and calorimetry techniques show that during water intrusion−extrusion cycles, significant variations occur in intruded volume, pressure, and heat when experiments last longer than ∼3 days. This suggests that the ZIF-8 material undergoes some structural and chemical modifications when it interacts with water under high pressure and for a sufficiently long time. These modifications could be attributed to the partial collapse of ZIF framework leading to a consequent decrease of pore volume. The formation of a small number of hydrophilic defects in ZIF-8 framework which facilitates water intrusion and thus leads to lower intrusion pressure and particular thermal effects could also be suspected. Such effects have been already observed for the intrusion of water in hydrophobic zeolites[55] and ZIFs.[31] In order to characterize changes in the host material structure provoked by the intrusion−extrusion of water under high pressure, various characterizations (XRD, N_2 sorption, SEM) of the ZIF-8 post-intruded materials have been employed and the obtained results are reported in the next sections.

3.2.3.1. X-Ray Diffraction

The XRD patterns of the samples before and after water intrusion−extrusion experiments with different durations are shown in Figure 3. Compared to the ZIF-8 parent pellet materials, the ZIF-8 structure is preserved in the case of the shortest experiment (9 h). However, 3 additional peaks of very low relative intensities at 11.06, 12.14, and 18.40° (2θ), with corresponding d-spacings of 8.00, 7.29, and 4.82 Å, appear for the experiments with the duration of 2 days and more. They do not correspond to the organic precursor, ZnO or $Zn(OH)_2$. In addition, they can not be assigned to ZIF-kat(Zn) or ZIF-L, some ZIF-8 polymorphs.[58−60] A concordance with diffraction peaks of ZIF-CO_3−1,[61] a hydrolysis residue of ZIF-8 often highlighted by Zhang et al.,[38−40] can be ruled out. On the other hand, these three peaks can be attributed to a crystallographic solution where $a = b = c \sim 34.05$ Å corresponds to a doubling of the lattice parameters of the conventional lattice. This means that the

ZIF-8 framework undergoes a disorder rather than a chemical alteration. Moreover, for the longer time experiments (4 and particularly 9 days), another crystalline phase is formed. This phase corresponds to ZIF-dia(Zn) phase (Figure 3), a denser polymorph of ZIF-8.[62, 63] The transformation of ZIF-8 in this dense phase explains well the decrease of intruded volume observed for the longest experiments. This partial transformation ZIF-8 → ZIF-dia(Zn) is irreversible in the conditions of our study and probably occurs by the partial transformation of parent material under the combined effect of high pressure and water exposure during intrusion−extrusion experiments. The experiments allow determining which factor is responsible for the observed ZIF-8 → ZIF-dia(Zn) phase transformation are presented in Section 3.3.

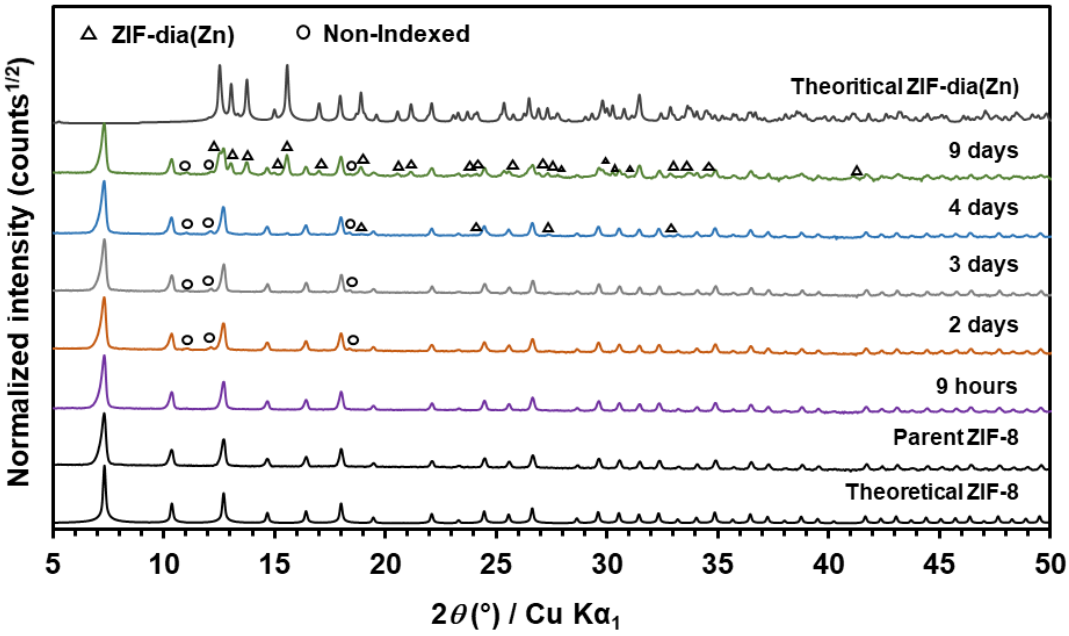

Figure 3. XRD patterns of simulated ZIF-8 and ZIF-dia (Zn), parent pellet sample, samples recovered after water intrusion−extrusion tests of different duration after 9 h and 2, 3, 4, and 9 days. Marks Δ correspond to ZIF-dia(Zn) and marks ○ highlight non-indexed peaks for conventional ZIF-8 unit-cell.

It is important to note that the same structural transformation of ZIF-8 is observed for the sample after calorimetric measurements (Figure S11). After one cycle of slow intrusion−extrusion experiment (12.5 days), XRD shows also that the ZIF-dia(Zn) phase starts to appear in the sample. Increase in the number of cycles to three (37.5 days) results in the formation of a significant amount of the same phase, but the sample is not completely transformed, indicating a rather low rate of structural transformation. Observation of the same transformation after analysis by the two different

techniques suggests that it is not an effect specific to a certain set of conditions, but a general phenomenon occurring when ZIF-8 is exposed to water under pressure.

3.2.3.2. Nitrogen Adsorption-Desorption at 77 K

Figure 4 represents nitrogen adsorption−desorption isotherms at 77 K of ZIF-8 materials after water intrusion−extrusion experiments by porosimetry (a and b) or calorimetry (c and d) for different durations. Except for the sample after the slow procedure calorimetry experiment with a duration of 37.5 days, all isotherms display hysteresis at low relative pressure characteristic of ZIF-8 solid.[52−54] Compared to the parent pellet material, the BET specific surface area of ZIF-8 samples decreases from 1361 to 1336, 1326, and 1314 $m^2 \cdot g^{-1}$ after 2, 3, and 4 days of experiments duration of water intrusion by porosimetry, respectively (Table 3). The microporous volume also decreases from 0.65 $cm^3 \cdot g^{-1}$ for the parent material to 0.64 and 0.63 $cm^3 \cdot g^{-1}$ after 2, 3, and 4 days of experiments duration under the same conditions, respectively. This decrease is significantly much more pronounced after 9 days of experiment. BET surface area and microporous volume fall down to 730 $m^2 \cdot g^{-1}$ and 0.35 $cm^3 \cdot g^{-1}$ in this case. The decrease of textural parameters is even more pronounced for the sample obtained after three cycles of slow procedure calorimetric experiments of a total duration of 37.5 days (Figure 4 and Table 3). For this sample, a BET surface of 161 $m^2 \cdot g^{-1}$ and a pore volume of 0.08 $cm^3.g^{-1}$ are obtained. This result can be explained by the partial transformation of ZIF-8 into the nonporous (dense) ZIF-dia(Zn) phase in agreement with XRD analysis.

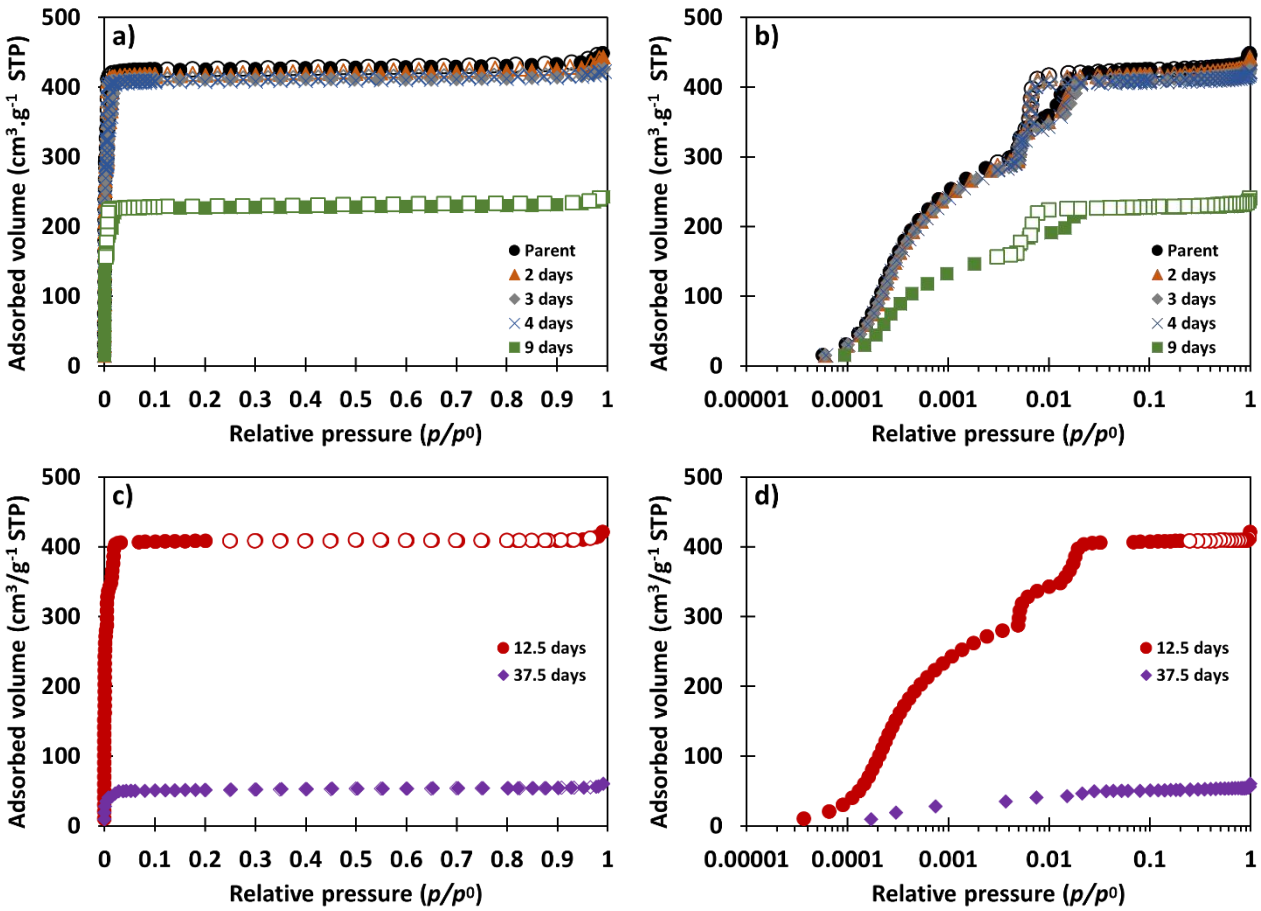

Figure 4. N_2 adsorption−desorption isotherms at 77 K of ZIF-8 parent sample (black) and the samples after water intrusion−extrusion by porosimetry with different experimental durations: (orange) after 2 days, (gray) after 3 days, (blue) after 4 days and (green) after 9 days; (red) after 12.5 days and (purple) after 37.5 days after calorimetry measurements. The plots are given with (a, c) a linear scale and (b, d) a logarithmic scale of the relative pressure. Filled and empty symbols correspond to the adsorption and desorption branches, respectively.

Table 3. Textural Properties of Post-Intruded ZIF-8 Samples with Different Experimental Durations, Microporous Volume (V_μ) and BET (S_{BET}) Surface of ZIF-8 Samples

Techniques	Experiments duration	Non-wetting liquid	S_{BET} ($m^2.g^{-1}$)	V_μ ($cm^3.g^{-1}$)
Porosimetry	**Parent Pellet**	/	1361	0.65
	9 hours	Water	1348	0.65
	2 days	Water	1336	0.64
	3 days	Water	1326	0.63
	4 days	Water	1314	0.63
	9 days	Water	730	0.35
Calorimetry	**Parent Powder**	/	1401	0.67
	12.5 days	Water	1301	0.63
	37.5 days	Water	161	0.08

3.2.3.3. Scanning Electron Microscopy

SEM images of ZIF-8 samples before and after water intrusion−extrusion tests are presented in Figure 5. SEM image for the parent ZIF-8 material exhibits the crystals of cubic shape with truncated edges which is expected for this type of synthesis.[48] The crystal size ranges from 350 to 1125 nm and with a median size of 550 nm. After 9 h or 2 days of water intrusion−extrusion tests, the ZIF-8 crystal morphology (shape and size) for the samples is similar to the parent pellet materials (Figure 5a−c). After 3 days of experiment duration, it is different as larger crystals (~3−5 μm) of different shapes start to form (Figure 5d). This can be ascribed to the formation of a new phase. After longer experiments (4 and 9 days) micrometric crystals of 7−10 μm, probably the ones of the new phase, seem to continue to grow while the small crystals lose their edges and their shape becomes less defined (Figure 5e,f). These results can be related to the formation of the ZIF-dia(Zn) phase and confirm the results obtained with XRD and nitrogen sorption.

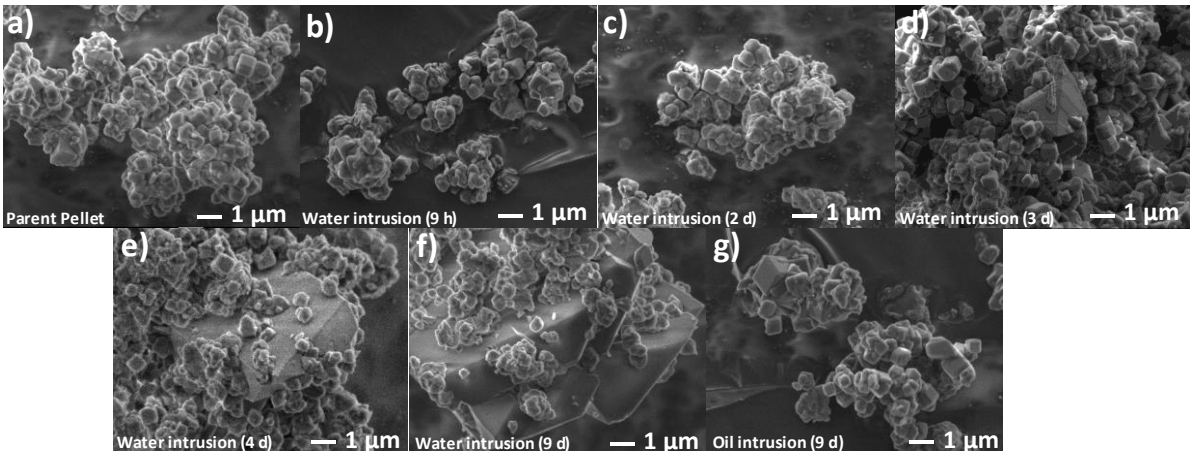

Figure 5. SEM images of (a) ZIF-8 parent sample and the samples after water intrusion−extrusion with different duration experiments, (b) after 9 h, (c) 2 days, (d) 3 days, (e) 4 days, (f) 9 days, and (g) 9 days of oil intrusion−extrusion.

3.3. Role of Different Factors in ZIF-8 Phase Transformation

ZIF-8 → ZIF-dia(Zn) transformation is an interesting phenomenon which deserves to be investigated more in detail. It can occur by two different ways: (a) solid-to-solid structure reorganization or (b) solid−liquid-solid trans-formation with partial hydrolysis of ZIF-8 leading to the formation of partially hydroxylated species followed by the condensation of these species to produce ZIF-dia(Zn). Whatever the mechanism is, this transformation requires the cleavage and formation of Zn−N bonds since the dia network contains only 6 membered rings whereas 4 and 6 membered rings are present

in the SOD structure of parent ZIF-8. In order to demonstrate the influence of water and pressure on this transformation, two separate studies of ZIF-8 stability were realized. The first one is based on compression−decompression cycles of ZIF-8 pellet with silicon oil as a nonwetting liquid under high pressure (up to 100 MPa) for 9 days as experimental duration. Since oil does not contain water, only the effect of mechanical compression can be considered. In the second experiment, a pellet of ZIF-8 is immersed in water for 12.5 days under atmospheric pressure. In this case, only the effect of water is assessed. According to XRD measurements, after both experiments, the structure of the ZIF-8 sample remains unchanged (Figures S12 and S13).

N_2 adsorption−desorption isotherms of ZIF-8 samples after 9 days of silicon oil compression under high pressure (by porosimetry) and after 12.5 days of immersion in water under atmospheric pressure have been compared with that of initial ZIF-8 (Figure S14). Only a slight or even negligible decrease is observed from 1361 to 1335 $m^2 \cdot g^{-1}$ and from 0.65 to 0.64 $cm^3 \cdot g^{-1}$ in terms of BET surface area and microporous volume, respectively, after silicon oil compression−decompression under high pressure tests (Table 4). Moreover, textural parameters for the sample after 12.5 days of contact with water under ambient conditions remain identical.

Table 4. Textural Properties of Parent Pellet ZIF-8, Post-Intruded ZIF-8 Sample with Silicon Oil, and ZIF-8 Sample Immersed in Water for 12.5 Days

Experiments duration	**Non-Wetting liquid**	S_{BET} **($m^2.g^{-1}$)**	V_μ **($cm^3.g^{-1}$)**
Parent Pellet	/	1361	0.65
9 days	Oil	1335	0.64
12.5 days	Water	1360	0.65

In order to complete the analyses, SEM images of ZIF-8 materials after 9 days of oil intrusion were recorded, and as expected, the shape and the crystal size of ZIF-8 materials are preserved (Figure 5g).

These results reveal that the ZIF-8 → ZIF-dia(Zn) transformation occurs under combined effects of water and high pressure. It can be therefore concluded that both water and pressure play each one a crucial role in ZIF-8 transformation. Accordingly, it could be assumed that ZIF-8 → ZIF-dia(Zn) transformation occurs in a two-step solid−liquid−solid way. First, partial hydrolysis of ZIF-8

framework takes place. Then the species, possibly from liquid phase, form the more thermodynamically stable dense ZIF-dia(Zn) phase.

The conclusion about the partial hydrolysis of ZIF-8 during its transformation into ZIF-dia(Zn) is surprising and raises a new question because of the absence of any hydrolysis products after water intrusion. Indeed, one can wonder why the hydrolysis mechanism of ZIF-8 does not go to completion giving for example $Zn(OH)_2$ and 2-methylimidazole (Hmim). The following thermodynamic argument can be advanced to explain this peculiar behavior. It can be calculated that the transformation of 1 mole of ZIF-8 (227.57 g) into 1 mole of ZIF-dia(Zn) produces a decrease in volume of the solid phase from 246.8 to 144.3 cm^3 given the densities of these two phases (0.92 $g \cdot cm^{-3}$ for ZIF-8[51] and 1.58 $g \cdot cm^{-3}$ for ZIF-dia(Zn)[62]). In contrast, the transformation of 1 mole of ZIF-8 through the hydrolysis into 1 mole of $Zn(OH)_2$ with a density of 3.09 $g \cdot cm^{-3}$,[64] and 2 moles of Hmim with a density of 1.14 $g \cdot cm^{-3}$,[65] would generate a volume of 176.5 cm^3. This calculation is a rough estimation but shows that the transformation of ZIF-8 into dia(Zn) yields a solid having a smaller volume than the hydrolysis products. Therefore, according to the Le Chatelier principle, under high pressure, the formation of ZIF-dia(Zn) is a thermodynamically favored process. We suggest thus that species with Zn−O bonds formed during water intrusion are intermediate and transient ones. Their formation allows possibly to decrease the activation energy of ZIF-8 → ZIF-dia(Zn) transformation.

4. Conclusions

The stability of the ZIF-8 phase during water intrusion−extrusion under high pressure (up to 100 MPa) has been studied by two complementary approaches: porosimetry and manometry coupled with calorimetry. For both techniques, the duration of measurements was varied in a wide range (3−900 h) in order to characterize the impact of this parameter on the stability of ZIF-8 and other parameters in relation to water intrusion. The post-intruded samples have been systematically characterized by XRD, N_2 adsorption−desorption at 77 K, and SEM. It is shown that the structural and textural properties of ZIF-8 are preserved if the duration of the measurements does not exceed ~3 days. Under these conditions, the water intrusion−extrusion process is fully reversible and the intrusion process is shown to be exothermic with heat of water/ZIF-8 interaction of −6.5 $J \cdot g^{-1}$. The latter result is in disagreement with previously published data suggesting an endothermic character of water intrusion in ZIF-8.[35]

If the duration of experiments involving water intrusion−extrusion in ZIF-8 is longer than ~3 days, a nonporous ZIF-dia(Zn) phase appears leading to lower surface area and microporous volume and poorer energetic performances of ZIF-8-based heterogeneous lyophobic systems. The process of transformation is, however, rather slow as it is not completed even after ~37.5 days of measurements. Additional experiments have evidenced that the combination of two factors, *i.e.*, high pressure and the presence of water, is required to trigger the observed transformation of ZIF-8 into ZIF-dia(Zn). Our findings demonstrate that the well-known porous ZIF-8 is not a thermodynamically stable phase in the presence of water under high pressure.

TOC Graphic

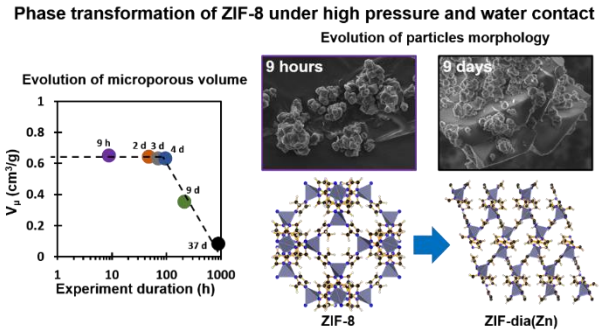
Phase transformation of ZIF-8 under high pressure and water contact
Evolution of particles morphology
Evolution of microporous volume
9 hours
9 days
1
0.8
0.6
0.4
0.2
0
V_μ (cm^3/g)
9 h
2 d
3 d
4 d
9 d
37 d
1
10
100
1000
Experiment duration (h)
ZIF-8
ZIF-dia(Zn)

Supporting information

The Supporting Information is available free of charge at https://pubs.acs.org/doi/10.1021/acs.jpcc.3c04290.

Scheme of the calorimetric setup; graphical description of fast and slow intrusion calorimetric procedures; XRD patterns of powder and pellet of ZIF-8; nitrogen adsorption−desorption isotherms at 77 K of ZIF-8 powder and pellet; TG curve of ZIF-8 powder; SEM image of ZIF-8 powder; pressure−volume diagrams of the “ZIF-8−water” systems from ZIF-8 powder and pellet with or without outgassing; XRD patterns of ZIF-8 powder and pellet with or without outgassing recovered after water intrusion−extrusion experiments; nitrogen adsorption−desorption isotherms at 77 K and textural data of ZIF-8 powder and pellet with or without outgassing recovered after water intrusion−extrusion experiments; heats of water/ZIF-8 interaction measured for three successive intrusion−extrusion cycles performed on the same sample; integral heat of water/solid interaction determined from slow intrusion experiments; XRD patterns of ZIF-8 samples recovered after fast and slow calorimetric procedures; XRD patterns of the ZIF-8 sample after 9 days in oil compression−decompression cycles under high pressure, and ZIF-8 sample after 12.5 days in water under atmospheric pressure; XRD patterns of ZIF-8 samples after water and oil intrusion−extrusion experiments (calorimetry setup); and nitrogen adsorption−desorption isotherms at 77 K of ZIF-8 samples after 9 days of oil compression−decompression experiments under high pressure and after 12.5 days in water under low pressure

Author information

Corresponding Authors
*(G. C.) E-mail gerald.chaplais@uha.fr; tel +33 389 33 68 87
*(I. B.) E-mail igor.bezverkhyy@u-bourgogne.fr; tel +33 380 39 60 38

Acknowledgements

The authors thank French National Research Agency for financial support to MESAMM project (ANR-19-CE05-0031)

References

(1) Clarke, L.; Edmonds, J.; Krey, V.; Richels, R.; Rose, S.; Tavoni, M. International Climate Policy Architectures: Overview of the EMF 22 International Scenarios. *Energy Econ.* **2009**, *31*, S64-S81 - 10.1016/j.eneco.2009.10.013

(2) Koohi-Fayegh, S.; Rosen, M. A. A Review of Energy Storage Types, Applications and Recent Developments. *J. Energy Storage* **2020**, *27*, 101047 - 10.1016/j.est.2019.101047

(3) Eroshenko, V. A. Unusual Properties of One Complex Thermodynamic System. *Dopov. Akad. Nauk Ukr. RSR, Ser. A: Fiz.-Tekh. Mat. Nauki* **1990**, 77-80 -

(4) Eroshenko, V. A. Hydrocapillary Accumulator. SU00943444, 04/28/1980, 1982.

(5) Eroshenko, V.; Regis, R. C.; Soulard, M.; Patarin, J. Energetics: A New Field of Applications for Hydrophobic Zeolites. *J. Am. Chem. Soc.* **2001**, *123*, 8129-8130 - 10.1021/ja011011a

(6) Tzanis, L.; Trzpit, M.; Soulard, M.; Patarin, J. High Pressure Water Intrusion Investigation of Pure Silica 1D Channel AFI, MTW And TON-Type Zeolites. *Microporous Mesoporous Mater.* **2011**, *146*, 119-126 - 10.1016/j.micromeso.2011.03.043

(7) Tzanis, L.; Nouali, H.; Daou, T. J.; Soulard, M.; Patarin, J. Influence of the Aqueous Medium on the Energetic Performances of Silicalite-1. *Mater. Lett.* **2014**, *115*, 229-232 - 10.1016/j.matlet.2013.10.063

(8) Ryzhikov, A.; Khay, I.; Nouali, H.; Daou, T. J.; Patarin, J. Energetic Performances of Pure Silica STF and MTT-type Zeolites under High Pressure Water Intrusion. *RSC Adv.* **2014**, *4*, 37655-37661 - 10.1039/c4ra05519e

(9) Ortiz, G.; Nouali, H.; Marichal, C.; Chaplais, G.; *Patarin, J.* Energetic performances of the metal-organic framework ZIF-8 obtained using high pressure water intrusion-extrusion experiments. *Phys. Chem. Chem. Phys.* **2013**, *15*, 4888-4891 - 10.1039/c3cp00142c

(10) Fraux, G.; Coudert, F.-X.; Boutin, A.; Fuchs, A. H. Forced Intrusion of Water and Aqueous Solutions In Microporous Materials: From Fundamental Thermodynamics to Energy Storage Devices. *Chem. Soc. Rev.* **2017**, *46*, 7421-7437 - 10.1039/c7cs00478h

(11) Pimentel, B. R.; Parulkar, A.; Zhou, E.-K.; Brunelli, N. A.; Lively, R. P. Zeolitic Imidazolate Frameworks: Next-Generation Materials for Energy-Efficient Gas Separations. *ChemSusChem* **2014**, *7*, 3202-3240 - 10.1002/cssc.201402647

(12) Park, K. S.; Ni, Z.; Côte, A. P.; Choi, J. Y.; Huang, R. D.; Uribe-Romo, F. J.; Chae, H. K.; O'Keeffe, M.; Yaghi, O. M. Exceptional Chemical and Thermal Stability of Zeolitic Imidazolate Frameworks. *Proc. Natl. Acad. Sci. USA* **2006**, *103*, 10186-10191 - 10.1073/pnas.0602439103

(13) Phan, A.; Doonan, C. J.; Uribe-Romo, F. J.; Knobler, C. B.; O'Keeffe, M.; Yaghi, O. M. Synthesis, Structure, and Carbon Dioxide Capture Properties of Zeolitic Imidazolate Frameworks. *Acc. Chem. Res.* **2010**, *43*, 58-67 - 10.1021/ar900116g

(14) Sumida, K.; Rogow, D. L.; Mason, J. A.; McDonald, T. M.; Bloch, E. D.; Herm, Z. R.; Bae, T.-H.; Long, J. R. Carbon Dioxide Capture in Metal-Organic Frameworks. *Chem. Rev.* **2011**, *112*, 724-781 - 10.1021/cr2003272

(15) Modak, A.; Jana, S. Advancement in Porous Adsorbents for Post-Combustion CO_2 Capture. *Microporous Mesoporous Mater.* **2019**, *276*, 107-132 - 10.1016/j.micromeso.2018.09.018

(16) Mason, J. A.; Veenstra, M.; Long, J. R. Evaluating Metal-Organic Frameworks for Natural Gas Storage. *Chem. Sci.* **2014**, *5*, 32-51 - 10.1039/c3sc52633j

(17) Suh, M. P.; Park, H. J.; Prasad, T. K.; Lim, D.-W. Hydrogen Storage in Metal-Organic Frameworks. *Chem. Rev.* **2011**, *112*, 782-835 - 10.1021/cr200274s

(18) Zhang, S.; Wang, J.; Zhang, Y.; Ma, J.; Huang, L.; Yu, S.; Chen, L.; Song, G.; Qiu, M.; Wang, X. Applications of Water-Stable Metal-Organic Frameworks in the Removal of Water Pollutants: a Review. *Environ. Pollut.* **2021**, *291*, 118076 - 10.1016/j.envpol.2021.118076

(19) Ighalo, J. O.; Rangabhashiyam, S.; Adeyanju, C. A.; Ogunniyi, S.; Adeniyi, A. G.; Igwegbe, C. A. Zeolitic Imidazolate Frameworks (ZIFs) for Aqueous Phase Adsorption - A Review. *J. Ind. Eng. Chem.* **2022**, *105*, 34-48 - 10.1016/j.jiec.2021.09.029

(20) Sun, Y.; Zhang, N.; Yue, Y.; Xiao, J.; Huang, X.; Ishag, A. Recent Advances in the Application of Zeolitic Imidazolate Frameworks (ZIFs) in Environmental Remediation: a Review. *Environ. Sci.: Nano* **2022**, *9*, 4069-4092 - 10.1039/d2en00601d

(21) Wang, H.; Luo, D.; Velasco, E.; Yu, L.; Li, J. Separation of Alkane and Alkene Mixtures by Metal-Organic Frameworks. *J. Mater. Chem. A* **2021**, *9*, 20874-20896 - 10.1039/d1ta04096k

(22) Melgar, V. M. A.; Kim, J.; Othman, M. R. Zeolitic Imidazolate Framework Membranes for Gas Separation: A Review Of Synthesis Methods And Gas Separation Performance. *J. Ind. Eng. Chem.* **2015**, *28*, 1-15 - 10.1016/j.jiec.2015.03.006

(23) Lu, G.; Hupp, J. T. Metal-Organic Frameworks as Sensors: A ZIF-8 Based Fabry-Perot Device as a Selective Sensor for Chemical Vapors and Gases. *J. Am. Chem. Soc.* **2010**, *132*, 7832-7833 - 10.1021/ja101415b

(24) Bhattacharjee, S.; Jang, M.-S.; Kwon, H.-J.; Ahn, W.-S. Zeolitic Imidazolate Frameworks: Synthesis, Functionalization, and Catalytic/Adsorption Applications. *Catal. Surv. Asia* **2014**, *18*, 101-127 - 10.1007/s10563-014-9169-8

(25) Yaghi, O. M.; O'Keeffe, M.; Ockwig, N. W.; Chae, H. K.; Eddaoudi, M.; Kim, J. Reticular Synthesis and the Design of New Materials. *Nature* **2003**, *423*, 705-714 - 10.1038/nature01650

(26) Ortiz, G.; Nouali, H.; Marichal, C.; Chaplais, G.; *Patarin, J.* Versatile energetic behavior of ZIF-8 upon high pressure intrusion-extrusion of aqueous electrolyte solutions. *J. Phys. Chem. C* **2014**, *118*, 7321-7328 - 10.1021/jp412354f

(27) Ortiz, G.; Nouali, H.; Marichal, C.; Chaplais, G.; *Patarin, J.* Energetic performances of "ZIF-71-aqueous solution" systems: a perfect shock-absorber with water. *J. Phys. Chem. C* **2014**, *118*, 21316-21322 - 10.1021/jp505484x

(28) Khay, I.; Chaplais, G.; Nouali, H.; Marichal, C.; *Patarin, J.* Water intrusion-extrusion experiments in ZIF-8: impacts of the shape and particle size on the energetic performances. *RSC Adv.* **2015**, *5*, 31514-31518 - 10.1039/c5ra02636a

(29) Khay, I.; Chaplais, G.; Nouali, H.; Ortiz, G.; Marichal, C.; *Patarin, J.* Assessment of the energetic performances of various ZIFs with SOD or RHO topology using high pressure water intrusion-extrusion experiments. *Dalton Trans.* **2016**, *45*, 4392-4400 - 10.1039/c5dt03486h

(30) Mortada, B.; Chaplais, G.; Veremeienko, V.; Nouali, H.; Marichal, C.; Patarin, J. Energetic Performances of ZIF-8 Derivatives: Impact of the Substitution (Me, Cl or Br) on Imidazolate Linker. *J. Phys. Chem. C* **2018**, *122*, 3846-3855 - 10.1021/acs.jpcc.7b08999

(31) Mortada, B.; Chaplais, G.; Nouali, H.; Marichal, C.; Patarin, J. Phase transformations of Metal-Organic Frameworks MAF-6 and ZIF-71 during intrusion-extrusion experiments. *J. Phys. Chem. C* **2019**, *123*, 4319-4328 - 10.1021/acs.jpcc.8b12047

(32) Sun, Y.; Rogge, S. M. J.; Lamaire, A.; Vandenbrande, S.; Wieme, J.; Siviour, C. R.; Van Speybroeck, V.; Tan, J.-C. High-rate nanofluidic energy absorption in porous zeolitic frameworks. *Nat. Mater.* **2021**, *20*, 1015-1023 - 10.1038/s41563-021-00977-6

(33) Zajdel, P.; Madden, D. G.; Babu, R.; Tortora, M.; Mirani, D.; Tsyrin, N. N.; Bartolome, L.; Amayuelas, E.; Fairen-Jimenez, D.; Lowe, A. R. *et al.* Turning Molecular Springs into Nano-Shock Absorbers: The Effect of Macroscopic Morphology and Crystal Size on the Dynamic Hysteresis of Water Intrusion-Extrusion into-from Hydrophobic Nanopores. *ACS Appl. Mater. Interfaces* **2022**, *14*, 26699-26713 - 10.1021/acsami.2c04314

(34) Michelin-Jamois, M.; Picard, C.; Vigier, G.; Charlaix, E. Giant Osmotic Pressure in the Forced Wetting of Hydrophobic Nanopores. *Phys. Rev. Lett.* **2015**, *115*, 036101 - 10.1103/PhysRevLett.115.036101

(35) Grosu, Y.; Renaudin, G.; Eroshenko, V. A.; Nedelec, J.-M.; Grolier, J.-P. E. Synergetic Effect of Temperature and Pressure on Energetic and Structural Characteristics of {ZIF-8 + Water} Molecular Spring. *Nanoscale* **2015**, *7*, 8803-8810 - 10.1039/c5nr01340b

(36) Liu, X.; Li, Y.; Ban, Y.; Peng, Y.; Jin, H.; Bux, H.; Xu, L.; Caro, J.; Yang, W. Improvement of Hydrothermal Stability of Zeolitic Imidazolate Frameworks. *Chem. Commun.* **2013**, *49*, 9140-9142 - 10.1039/c3cc45308a

(37) James, J. B.; Lin, Y. S. Kinetics of ZIF-8 Thermal Decomposition in Inert, Oxidizing, and Reducing Environments. *J. Phys. Chem. C* **2016**, *120*, 14015-14026 - 10.1021/acs.jpcc.6b01208

(38) Zhang, H.; Liu, D.; Yao, Y.; Zhang, B.; Lin, Y. S. Stability of ZIF-8 Membranes and Crystalline Powders in Water at Room Temperature. *J. Membr. Sci.* **2015**, *485*, 103-111 - 10.1016/j.memsci.2015.03.023

(39) Zhang, H.; Zhao, M.; Lin, Y. S. Stability of ZIF-8 in Water under Ambient Conditions. *Microporous Mesoporous Mater.* **2019**, *279*, 201-210 - 10.1016/j.micromeso.2018.12.035

(40) Zhang, H.; Zhao, M.; Yang, Y.; Lin, Y. S. Hydrolysis and Condensation of ZIF-8 in Water. *Microporous Mesoporous Mater.* **2019**, *288*, 109568 - 10.1016/j.micromeso.2019.109568

(41) Moggach, S. A.; Bennett, T. D.; Cheetham, A. K. The Effect of Pressure on ZIF-8: Increasing Pore Size with Pressure and the Formation of a High-Pressure Phase at 1.47 GPa. *Angew. Chem., Int. Ed.* **2009**, *48*, 7087-7089 - 10.1002/anie.200902643

(42) Choi, J.; Im, J.; Noh, K.; Kim, J.; Vogt, T.; Lee, Y. Universal Gas-Uptake Behavior of a Zeolitic Imidazolate Framework ZIF-8 at High Pressure. *J. Phys. Chem. C* **2019**, *123*, 25769-25774 - 10.1021/acs.jpcc.9b08539

(43) Im, J.; Yim, N.; Kim, J.; Vogt, T.; Lee, Y. High-pressure Chemistry of a Zeolitic Imidazolate Framework compound in the presence of different fluids. *J. Am. Chem. Soc.* **2016**, *138*, 11477-11480 - 10.1021/jacs.6b07374

(44) Coiffard, L.; Eroshenko, V. A.; Grolier, J.-P. E. Thermomechanics of the Variation of Interfaces in Heterogeneous Lyophobic Systems. *AIChE J.* **2005**, *51*, 1246-1257 - 10.1002/aic.10371

(45) Karbowiak, T.; Paulin, C.; Bellat, J.-P. Determination of Water Intrusion Heat in Hydrophobic Microporous Materials by High Pressure Calorimetry. *Microporous Mesoporous Mater.* **2010**, *134*, 8-15 - 10.1016/j.micromeso.2010.05.001

(46) Karbowiak, T.; Weber, G.; Bellat, J.-P. Confinement of Water in Hydrophobic Nanopores: Effect of the Geometry on the Energy of Intrusion. *Langmuir* **2014**, *30*, 213-219 - 10.1021/la4043183

(47) Karbowiak, T.; Paulin, C.; Ballandras, A.; Weber, G.; Bellat, J.-P. Thermal Effects of Water Intrusion in Hydrophobic Nanoporous Materials. *J. Am. Chem. Soc.* **2009**, *131*, 9898-9899 - 10.1021/ja903954h

(48) He, M.; Yao, J.; Liu, Q.; Wang, K.; Chen, F.; Wang, H. Facile Synthesis of Zeolitic Imidazolate Framework-8 from a Concentrated Aqueous Solution. *Microporous Mesoporous Mater.* **2014**, *184*, 55-60 - 10.1016/j.micromeso.2013.10.003

(49) Walton, K. S.; Snurr, R. Q. Applicability of the BET method for determining surface areas of microporous metal-organic frameworks. *J. Am. Chem. Soc.* **2007**, *129*, 8552-8556 - 10.1021/ja071174k

(50) Trzpit, M.; Soulard, M.; Patarin, J. The Pure Silica Chabazite: A High Volume Molecular Spring at Low Pressure for Energy Storage. *Chem. Lett.* **2007**, *36*, 980-981 - 10.1246/cl.2007.980

(51) Saint Remi, J. C.; Rémy, T.; Van Hunskerken, V.; van de Perre, S.; Duerinck, T.; Maes, M.; De Vos, D.; Gobechiya, E.; Kirschhock, C. E. A.; Baron, G. V. *et al.* Biobutanol Separation with the Metal–Organic Framework ZIF-8. *ChemSusChem* **2011**, *4*, 1074-1077 - 10.1002/cssc.201100261

(52) Fairen-Jimenez, D.; Moggach, S. A.; Wharmby, M. T.; Wright, P. A.; Parsons, S.; Düren, T. Opening the Gate: Framework Flexibility in ZIF-8 Explored by Experiments and Simulations. *J. Am. Chem. Soc.* **2011**, *133*, 8900-8902 - 10.1021/ja202154j

(53) Ania, C. O.; García-Pérez, E.; Haro, M.; Gutiérrez-Sevillano, J. J.; Valdés-Solís, T.; Parra, J. B.; Calero, S. Understanding Gas-Induced Structural Deformation of ZIF-8. *J. Phys. Chem. Lett.* **2012**, *3*, 1159-1164 - 10.1021/jz300292y

(54) Chaplais, G.; Fraux, G.; Paillaud, J.-L.; Marichal, C.; Nouali, H.; Fuchs, A. H.; Coudert, F.-X.; Patarin, J. Impacts of the Imidazolate Linker Substitution (CH_3, Cl, or Br) on the Structural and Adsorptive Properties of ZIF-8. *J. Phys. Chem. C* **2018**, *122*, 26945-26955 - 10.1021/acs.jpcc.8b08706

(55) Kabalan, I.; Khay, I.; Nouali, H.; Ryzhikov, A.; Lebeau, B.; Albrecht, S.; Rigolet, S.; Fadlallah, M.-B.; Toufaily, J.; Hamieh, T. *et al.* Influence of the Particle Sizes on the Energetic Performances of MFI-Type Zeolites. *J. Phys. Chem. C* **2015**, *119*, 18074-18083 - 10.1021/acs.jpcc.5b04484

(56) Sun, Y.; Li, Y.; Tan, J.-C. Framework Flexibility of ZIF-8 under Liquid Intrusion: Discovering Time-Dependent Mechanical Response and Structural Relaxation. *Phys. Chem. Chem. Phys.* **2018**, *20*, 10108-10113 - 10.1039/c8cp00447a

(57) Tortora, M.; Zajdel, P.; Lowe, A. R.; Chorazewski, M.; Leao, J. B.; Jensen, G. V.; Bleuel, M.; Giacomello, A.; Casciola, C. M.; Meloni, S. *et al.* Giant Negative Compressibility by Liquid Intrusion into Superhydrophobic Flexible Nanoporous Frameworks. *Nano Lett.* **2021**, *21*, 2848-2853 - 10.1021/acs.nanolett.0c04941

(58) Chen, R.; Yao, J.; Gu, Q.; Smeets, S.; Baerlocher, C.; Gu, H.; Zhu, D.; Morris, W.; Yaghi, O. M.; Wang, H. A Two-Dimensional Zeolitic Imidazolate Framework with a Cushion-Shaped Cavity for CO_2 Adsorption. *Chem. Commun.* **2013**, *49*, 9500-9502 - 10.1039/c3cc44342f

(59) Lo, Y.; Lam, C. H.; Chang, C.-W.; Yang, A.-C.; Kang, D.-Y. Polymorphism/Pseudopolymorphism of Metal-Organic Frameworks Composed of Zinc(Ii) and 2-Methylimidazole: Synthesis, Stability, and Application in Gas Storage. *RSC Adv.* **2016**, *6*, 89148-89156 - 10.1039/c6ra19437k

(60) Katsenis, A. D.; Puškarić, A.; Štrukil, V.; Mottillo, C.; Julien, P. A.; Užarević, K.; Pham, M.-H.; Do, T.-O.; Kimber, S. A. J.; Lazić, P. *et al.* In Situ X-Ray Diffraction Monitoring of a Mechanochemical Reaction Reveals a Unique Topology Metal-Organic Framework. *Nat. Commun.* **2015**, *6*, 6662 - 10.1038/ncomms7662

(61) Basnayake, S. A.; Su, J.; Zou, X.; Balkus, K. J., Jr. Carbonate-Based Zeolitic Imidazolate Framework for Highly Selective CO_2 Capture. *Inorg. Chem.* **2015**, *54*, 1816-1821 - 10.1021/ic5027174

(62) Shi, Q.; Chen, Z.; Song, Z.; Li, J.; Dong, J. Synthesis of ZIF-8 and ZIF-67 by Steam-Assisted Conversion and an Investigation of Their Tribological Behaviors. *Angew. Chem., Int. Ed.* **2011**, *50*, 672-675 - 10.1002/anie.201004937

(63) Zhu, A.-X.; Lin, R.-B.; Qi, X.-L.; Liu, Y.; Lin, Y.-Y.; Zhang, J.-P.; Chen, X.-M. Zeolitic Metal Azolate Frameworks (MAFs) from ZnO/$Zn(OH)_2$ and Monoalkyl-Substituted Imidazoles and 1,2,4-Triazoles: Efficient Syntheses and Properties. *Microporous Mesoporous Mater.* **2012**, *157*, 42-49 - 10.1016/j.micromeso.2011.11.033

(64) Stahl, R.; Jung, C.; Lutz, H. D.; Kockelmann, W.; Jacobs, H. Crystal Structures and Hydrogen Bonding for ε-$Be(OH)_2$ and ε-$Zn(OH)_2$. *Z. Anorg. Allg. Chem.* **1998**, *624*, 1130-1136 - 10.1002/(SICI)1521-3749(199807)624:7<1130::AID-ZAAC1130>3.0.CO;2-G

(65) Serpell, C. J.; Beer, P. D. Intermolecular Interactions in Bromo-, Methyl-, and Cyanoimidazole Derivatives. *Cryst. Growth Des.* **2013**, *13*, 2866-2871 - 10.1021/cg400273p